7

Single Mode Operation of 1.5-μm Waveguide Optical Isolators Based on the Nonreciprocal-loss Phenomenon

T. Amemiya[1] and Y. Nakano[2]
[1]*Quantum Nanoelectronics Research Center, Tokyo Institute of Technology,*
[2]*Research Center for Advanced Science and Technology, University of Tokyo, Japan*

1. Introduction

The explosive growth of Internet traffic requires the development of advanced optical telecommunication networks that can enable the high-speed processing of this exponentially growing data traffic. Such advanced network systems will need an enormous number of optical devices, so photonic integrated circuits (PICs) are indispensable for constructing the system at low cost, reduced space, and high reliability. To date, monolithic integration on an indium phosphide (InP) substrate is the most promising way of making PICs because it has the capability to integrate both active and passive optical functions required in optical transport systems for the 1.3-um or 1.55-um telecom window. To develop large-scale, InP-based monolithic PICs, various planar optical devices such as lasers, modulators, detectors, multiplexers/demultiplexers, and optical amplifiers have been developed [1-4].

This paper provides an overview of the present state of research on waveguide optical isolators for InP-based monolithic PICs. Optical isolators are indispensable elements of PICs used to interconnect different optical devices while avoiding the problems caused by undesired reflections of light in the circuit. They must have the form of a planar waveguide because they must be monolithically combined with other semiconductor-waveguide-based optical devices such as lasers, amplifiers, and modulators. Conventional isolators cannot meet this requirement because they use Faraday rotators and polarizers, which are difficult to integrate with waveguide-based semiconductor optical devices. For this reason, many efforts have been expended in developing waveguide isolators [5-11]. Although the research on waveguide isolators is still in the experimental stage, it will probably reach a level of producing practical devices in the near future.

In Section 2, we first give a short sketch of conventional optical isolators. The conventional isolator is a mature device made with established technology and has sufficient performance (low insertion loss and large isolation ratio) for use in optical transport systems. However, it uses bulky components, a Faraday rotator and polarizers, and therefore cannot be used in PICs. We then turn to waveguide optical isolators and, in Section 3, outline two promising methods of making waveguide isolators on InP substrates. All of the methods use semiconductor optical waveguides combined with magnetic materials. One of them is based on the polarization conversion of light caused by the Faraday effect; another is based on a

Source: Advances in Optical and Photonic Devices, Book edited by: Ki Young Kim,
ISBN 978-953-7619-76-3, pp. 352, January 2010, INTECH, Croatia, downloaded from SCIYO.COM

nonreciprocal phase shift in a waveguide interferometer; the third is based on nonreciprocal propagation loss in a magneto-optic waveguide. In the succeeding sections, we focus on the nonreciprocal-loss waveguide isolator and make a detailed explanation of the isolator. In Section 4, we explain the principle and theory of the nonreciprocal-loss phenomenon. Actual devices based on this phenomenon have been developed. In Sections 5, we report the experimental results for the devices consisting of semiconductor optical waveguides combined with manganese arsenide (MnAs), which are ferromagnetic material compatible with semiconductor manufacturing process. We hope that this paper will be helpful to readers who are aiming to develop photonic integrated circuits.

2. Conventional optical isolator

Optical isolators are one of the most important passive components in optical communication systems. The function of an optical isolator is to let a light beam pass through in one direction, that is, the forward direction only, like a one-way traffic. Optical isolators are used to prevent destabilizing feedback of light that causes undesirable effects such as frequency instability in laser sources and parasitic oscillation in optical amplifiers.
Ordinary optical isolators available commercially make use of the Faraday effect to produce nonreciprocity. The Faraday effect is a magneto-optic phenomenon in which the polarization plane of light passing through a transparent substance is rotated in the presence of a magnetic field parallel to the direction of light propagation. The Faraday effect occurs in many solids, liquids, and gases. The magnitude of the rotation depends on the strength of the magnetic field and the nature of the transmitting substance. Unlike in the optical activity (or natural activity), the direction of the rotation changes its sign for light propagating in reverse. For example, if a ray traverses the same path twice in opposite directions, the total rotation is double the rotation for a single passage. The Faraday effect is thus non-reciprocal.

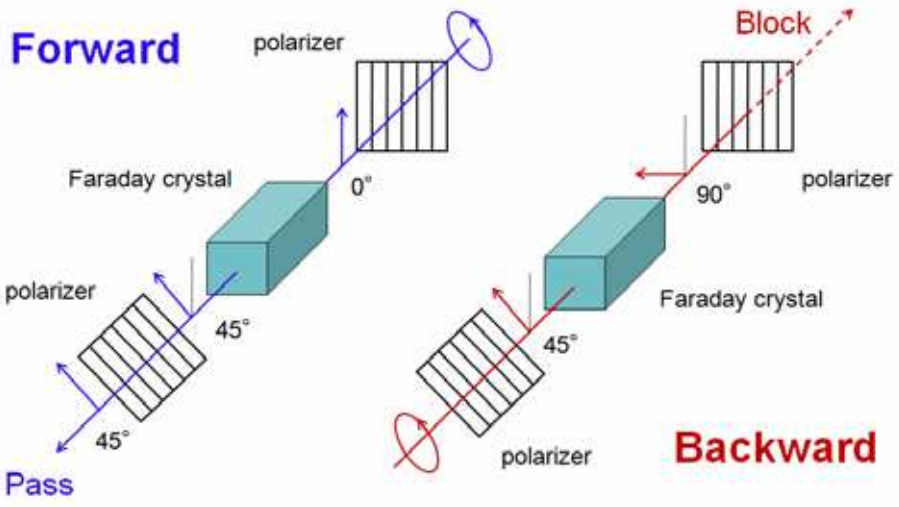

Fig. 1. Schematic structure of ordinary optical isolator.

Figure 1 shows the schematic structure of an ordinary optical isolator. The isolator consists of three components, i.e., a Faraday rotator, an input polarizer, and an output polarizer. The Faraday rotator consists of a magnetic garnet crystal such as yttrium iron garnet and terbium gallium garnet placed in a cylindrical permanent magnet and rotates the polarization of passing light by 45°. As illustrated in Fig. 1, light traveling in the forward direction (from A to B) will pass through the input polarizer and become polarized in the vertical plane (indicated by Pi). On passing through the Faraday rotator, the plane of polarization will be rotated 45° on axis. The output polarizer, which is aligned 45° relative to the input polarizer, will then let the light pass through. In contrast, light traveling in the reverse direction (from B to A) will pass through the output polarizer and become polarized by 45° (indicated by Pr). The light will then pass through the Faraday rotator and experience additional 45° of non-reciprocal rotation. The light is now polarized in the horizontal plane and will be rejected by the input polarizer, which allows light polarized in the vertical plane to pass through.
The ordinary optical isolator is bulky (therefore called a bulk isolator) and incompatible with waveguide-based optical devices, so it cannot be used in PICs. It has, however, superior optical characteristics (low forward loss and high backward loss) as shown in Fig. 2 [12]. Such good performance is a target in developing waveguide optical isolators.

Optical Component	Free Space Optical Isolator		unit
Structure	Single	Double	
Center Wavelength	1310, 1480, and 1550		[nm]
Insertion Loss	≦0.3	≦0.6	[dB]
Backward Loss	≧30	≧50	[dB]
Outer Diameter	ϕ3		[mm]
Length	1.5	NA	[mm]
Tilt	6		[deg.]
Clear Aperture	ϕ0.8	ϕ0.75	[mm]

Fig. 2. Optical characteristics of ordinary isolators available commercially [12]

3. Recent progress in waveguide optical isolators

3.1 How to make waveguide optical isolators

There are several strategies to develop waveguide optical isolators that can be integrated monolithically with waveguide-based semiconductor optical devices on an InP substrate. The strategies can be classified into two types. One is to use the Faraday effect as in conventional bulk isolators. Transferring the principle of bulk isolators to a planer waveguide geometry raises a number of inherent difficulties such as the discoherence of polarization rotation induced by structural birefringence. Therefore new idea is needed to use the Faraday effect in waveguide structure. Sophisticated examples are the Cotton-Mouton isolator [13, 14] and the quasi-phase-matching (QPM) Faraday rotation isolator [15, 16]. The latter in particular have attracted attention in recent years because of its compact techniques for producing the device. The other strategy to make waveguide isolators is to use asymmetric magneto-optic effects that occur in semiconductor waveguides combined with magnetic material. Leading examples are the nonreciprocal-phase-shift isolator [17-20] and the nonreciprocal-loss isolator [21-26]. The nonreciprocal-loss isolator uses no rare-earth garnet, so it is very compatible with standard semiconductor manufacturing processes. In

the following sections, we give the outline of the QPM Faraday rotation isolator and the nonreciprocal-phase-shift isolator. The nonreciprocal-loss isolator, which has been developed in our laboratory, is explained in detail in Section 4.

3.2 Quasi-phase-matching faraday rotation isolator

Figure 3 shows a schematic of the QPM Faraday rotation isolator. The device consists of a Faraday rotator (non-reciprocal) section and a polarization rotator (reciprocal) section integrated with a semiconductor laser diode that provides an TE-polarized output. The Faraday rotator section consists of an AlGaAs/GaAs waveguide combined with a sputter-coated film of magnetic rare-earth garnet $CeY_2Fe_5O_x$. To obtain an appropriate polarization rotation, this device uses the QPM Faraday effect in an upper-cladding that periodically alternates between magneto-optic (MO) and non-MO media. Incident light of TE mode traveling in the forward direction will first pass through the Faraday rotator section to be rotated by +45°. The light then passes through the reciprocal polarization rotator section and is rotated by -45°. Consequently, the light keeps its TE mode and passes through the output edge. In contrast, backward traveling light of TE mode from the output filter is first rotated by +45° in the reciprocal polarization rotator and then nonreciprocally rotated by +45° in the Faraday rotator section. Consequently, backward light is transformed into a TM mode and therefore has no influence on the stability of the laser because the TE-mode laser diode is insensitive to TM-polarised light. The point of this device is TE-TM mode conversion in the waveguide. At the present time, efficient mode conversion cannot be achieved, so practical devices have yet to be developed.

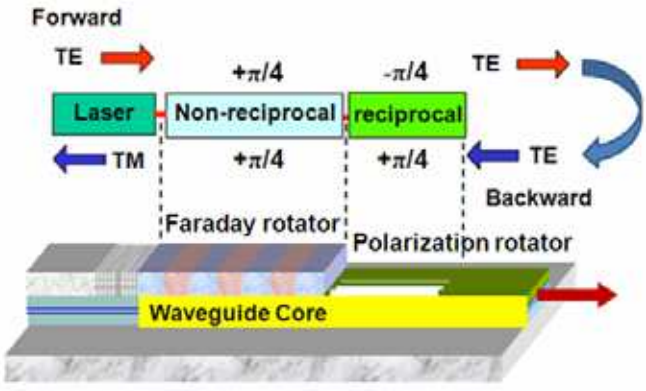

Fig. 3. Schematic of QPM Faraday rotation isolator.

Using magneto-optical waveguides made of $Cd_{1-x}Mn_xTe$ is effective to achieve efficient mode conversion [27, 28]. Diluted magnetic semiconductor $Cd_{1-x}Mn_xTe$ has the zincblende crystal structure, the same as that of ordinary electro-optical semiconductors such as GaAs and InP. Therefore, a single crystalline $Cd_{1-x}Mn_xTe$ film can be grown epitaxially on GaAs and InP substrates. In addition, $Cd_{1-x}Mn_xTe$ exhibits a large Faraday effect near its absorption edge because of the anomalously strong exchange interaction between the *sp*-band electrons and localized *d* electrons of Mn2+. Almost complete TE-TM mode conversion (98%+/-2% conversion) was observed in a $Cd_{1-x}Mn_xTe$ waveguide layer on a GaAs substrate [27, 28].

3.3 Nonreciprocal phase-shift isolator

The nonreciprocal-phase-shift isolator uses a modified Mach-Zehnder interferometer that is designed so that light waves traveling in two arms will be in-phase for forward propagation and out-of-phase for backward propagation. Figure 4 shows the structure of the isolator combined with a laser. The InGaAsP Mach-Zehnder interferometer consists of a pair of three-guide tapered couplers, and an ordinary reciprocal 90° shifter on one of the arms. Reciprocal phase shifting is achieved simply by setting a difference in dimensions or a refractive index between the optical paths along two arms. A magnetic rare-earth garnet YIG:Ce layer is placed on the arms to form a nonreciprocal 90° phase shifter on each arm. The garnet layer was pasted on the interferometer by means of a direct-bonding technique. Two external magnetic fields are applied to the magnetic layer on the two arms in an anti-parallel direction, as shown in Fig. 4; this produces a nonreciprocal phase shift in the interferometer in a push-pull manner. The isolator operates as follows. A forward-traveling light wave from the laser enters the central waveguide of the input coupler and divided between the two arms. During the light wave traveling in the arms, a -90° nonreciprocal phase difference is produced, but it is canceled by a +90° reciprocal phase difference. The divided two waves recouple at the output coupler, and output light will appear in the central waveguide. In contrast, for a backward-traveling wave from the output coupler, the nonreciprocal phase difference changes its sign to +90°, and it is added to the reciprocal phase difference to produce a total difference of 180°. Consequently, output light will appear in the two waveguides on both sides of the input coupler and not appear in the central waveguide.

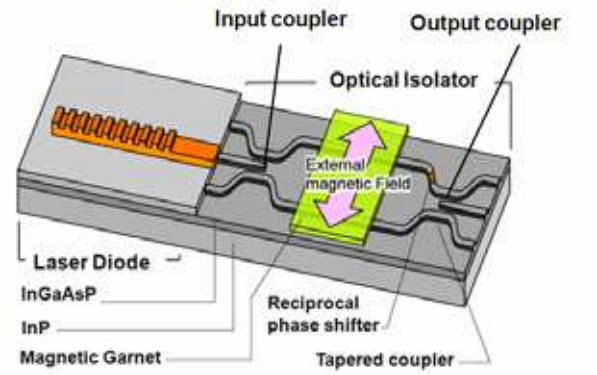

Fig. 4. Nonreciprocal-phase-shift isolator uses modified Mach-Zehnder interferometer.

4. Nonreciprocal loss phenomenon in magneto-optic waveguides

4.1 What is nonreciprocal loss phenomenon

One of the promising ways of creating waveguide optical isolators is by making use of the phenomenon of nonreciprocal loss. This phenomenon is a nonreciprocal magneto-optic phenomenon where——in an optical waveguide with a magnetized metal layer——the propagation loss of light is larger in backward than in forward propagation. Using this phenomenon can provide new waveguide isolators that use neither Faraday rotator nor polarizer and, therefore, are suitable for monolithic integration with other optical devices on

an InP substrate. The theory of the nonreciprocal loss phenomenon was first proposed by Takenaka, Zaets, and others in 1999 [29, 30]. After that, Ghent University-IMEC and Alcatel reported leading experimental results in 2004; they made an isolator consisting of an InGaAlAs/InP semiconductor waveguide combined with a ferromagnetic CoFe layer for use at 1.3-μm wavelength [21, 22]. Inspired by this result, aiming to create polarization-insensitive waveguide isolators for 1.5-μm-band optical communication systems, we have been developing both TE-mode and TM-mode isolators based on this phenomenon. We built prototype devices and obtained a nonreciprocity of 14.7 dB/mm for TE-mode devices and 12.0 dB/mm for TM-mode devices——to our knowledge, the largest values ever reported for 1.5-μm-band waveguide isolators. The TE-mode device consisted of an InGaAsP/InP waveguide with a ferromagnetic Fe layer attached on a side of the waveguide [24]. For the TM-mode device, instead of ordinary ferromagnetic metals, we used ferromagnetic intermetallic compounds MnAs and MnSb, which are very compatible with semiconductor manufacturing processes. The following sections provide the details on this TM-mode isolator.

4.2 Structure of the TM-mode waveguide isolator

Figure 5 illustrates our TM-mode waveguide isolators with a cross section perpendicular to the direction of light propagation. Two kinds of structure are shown. The device consists of a magneto-optical planar waveguide that is composed of a TM-mode semiconductor optical-amplifying waveguide (SOA waveguide) on an InP substrate and a ferromagnetic layer attached on a top of the waveguide. To operate the SOA, a metal electrode is put on the surface of the ferromagnetic layer (a driving current for the SOA flows from the electrode to the substrate). Incident light passes through the SOA waveguide perpendicular to the figure (z-direction). To operate the device, an external magnetic field is applied in the x-direction so that the ferromagnetic layer is magnetized perpendicular to the propagation of light. Light traveling along the waveguide interacts with the ferromagnetic layer.

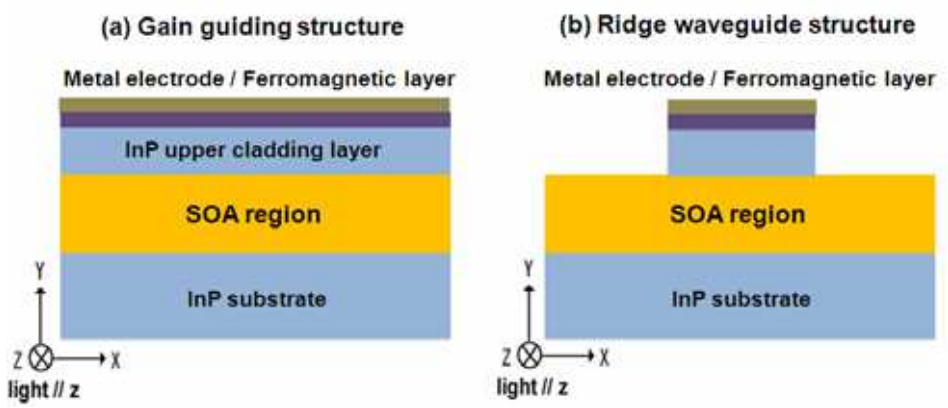

Fig. 5. Typical TM-mode nonreciprocal-loss waveguide isolators.

The nonreciprocal propagation loss is caused by the magneto-optic transverse Kerr effect in the magneto-optical planar waveguide. To put it plainly for TM-mode light, the nonreciprocity is produced when light is reflected at the interface between the magnetized

ferromagnetic layer and the SOA waveguide. The light reduces its intensity when reflected from the ferromagnetic layer, which absorbs light strongly, and the reduction is larger for backward propagating light than forward propagating light because of the transverse Kerr effect. As a result, the propagation loss is larger for backward propagation (-z-direction) than for forward propagation (z-direction). Figure 6 illustrates the operation of the isolator on the propagation constant plane of the waveguide. The backward light is attenuated more strongly than forward light. Since forward light is also attenuated, the SOA is used to compensate for the forward loss; the SOA is operated so that the net loss for forward propagation will be zero. Under these conditions, the waveguide can act as an optical isolator.

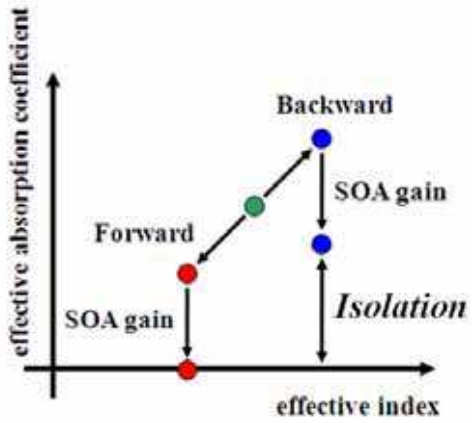

Fig. 6. Principle of nonreciprocal-loss waveguide isolator.

4.3 Theory of nonreciprocal loss in the waveguide isolator

Let us calculate the nonreciprocal loss in the magneto-optic waveguide and design optimized structure for the isolator device, using electromagnetic simulation. In the TM-mode isolator, light traveling along the SOA waveguide extends through the cladding layer into the ferromagnetic layer to a certain penetration depth and interacts with magnetization vector in the ferromagnetic layer (see Fig. 5). Therefore, the thicknesses of the cladding layer and the ferromagnetic layer greatly affect the performance—the isolation ratio and forward loss (insertion loss) —of the isolator as follows:

i. A large isolation ratio can be obtained at small cladding-layer thickness because a thin cladding layer easily lets light through into the ferromagnetic layer to produce a large magneto-optic interaction. Therefore, the cladding layer has to be thin as long as the amplifying gain of the SOA can compensate for the absorption loss of light in the ferromagnetic layer.
ii. The ferromagnetic layer has to be thicker than its penetration depth of light. If it is not, light leaks out of the upper part of the ferromagnetic layer and is needlessly absorbed by the metal electrode. This reduces the isolation ratio because part of the propagating light in the device cannot interact with the ferromagnetic layer.

To determine the optimum thicknesses of the cladding and ferromagnetic layers, we calculated the isolation ratio and the insertion loss of the device as a function of the

thicknesses by means of two-dimensional electromagnetic simulation based on the finite difference method (FDM).
In this device, the structure of the SOA has an influence on the device performance as well. However, the SOA structure cannot be changed greatly under the condition that the SOA should amplify TM-mode light at 1.5-μm-band wavelength. Therefore, we focus only on the thicknesses of the cladding and ferromagnetic layers to optimize the device performance.
The nonreciprocity of the device is caused by the off-diagonal elements in the dielectric tensor of the ferromagnetic layer. The dielectric tensor of each layer in the device is given by

$$\tilde{\varepsilon}_n = \begin{pmatrix} \varepsilon_n & 0 & 0 \\ 0 & \varepsilon_n & j\alpha \\ 0 & -j\alpha & \varepsilon_n \end{pmatrix}, \tag{3-1}$$

where ε_n is the diagonal element of the tensor in nth layer. The off-diagonal element α is 0 except in the ferromagnetic layer. Using these tensors, we write the Maxwell's equations in an isotropic charge-free medium as

$$\begin{aligned} \nabla \times \mathbf{H} &= j\omega\varepsilon_0 \tilde{\varepsilon}_n \mathbf{E} \\ \nabla \times \mathbf{E} &= -j\omega\mu_0 \mathbf{H} \\ \nabla \cdot (\tilde{\varepsilon}_n \mathbf{E}) &= 0 \end{aligned}. \tag{3-2}$$

Taking the rot of the second equation and using the first equation, we obtain the equation,

$$\nabla(\nabla \cdot \mathbf{E}) - \nabla^2 \mathbf{E} = k_0{}^2 \tilde{\varepsilon}_n \mathbf{E}, \tag{3-3}$$

where we used $\nabla \times (\nabla \times \mathbf{E}) = \nabla(\nabla \cdot \mathbf{E}) - \nabla^2 \mathbf{E}$, and $k_0 = \omega\sqrt{\mu_0\varepsilon_0} = 2\pi/\lambda$ is the free-space propagation constant. Using the second and third equations in (3-2) and $\partial_z = j\beta$, the z component of eq. (3-3) can be written as

$$\partial_x{}^2 E_z + \partial_y{}^2 E_z + (k_0{}^2 \varepsilon_n - \beta^2) E_z = j\alpha k_0{}^2 E_y - \frac{\alpha\omega\mu_0}{\varepsilon_n} \partial_z H_x, \tag{3-4}$$

where β is the propagation constant in the device along z direction, E_t and H_t (t = x, y, z) are electric field (parallel to t axis) and magnetic field (parallel to t axis) of the light.
The y and z components of the first equation in (3-2) can be given by the equations for TM-mode light ($E_x = H_y = H_z = 0$),

$$\begin{aligned} \partial_z H_x &= -\alpha\omega\varepsilon_0 E_z + j\omega\varepsilon_0 \varepsilon_n E_y \\ -\partial_y H_x &= \alpha\omega\varepsilon_0 E_y + j\omega\varepsilon_0 \varepsilon_n E_z \end{aligned}. \tag{3-5}$$

Substituting the first equation of (3-5) into eq. (3-4) gives the equation for E_z,

$$\partial_x{}^2 E_z + \partial_y{}^2 E_z + \left(k_0{}^2 \varepsilon_n - \beta^2 - \frac{k_0{}^2 \alpha^2}{\varepsilon_n} \right) E_z = 0. \tag{3-6}$$

Using eqs. (3-5), we can express E_z with H_x as

$$E_z = \frac{j\varepsilon_n}{\omega\varepsilon_0(\varepsilon_n{}^2 - \alpha^2)}\left(\partial_y H_x - \frac{\alpha\beta}{\varepsilon_n}H_x\right). \tag{3-7}$$

From eqs. (3-6) and (3-7), we can obtain the scalar wave equation for magnetic field H_x of TM waves in each layer. The wave equation in non-magnetic layers (α=0) is given by

$$\partial_x{}^2 H_x + \partial_y{}^2 H_x + \phi H_x = 0 \quad (\phi = k_0{}^2\varepsilon_n - \beta^2)\,. \tag{3-8}$$

For the ferromagnetic layer, the wave equation has first-order and third-order derivative terms because of the nonzero off-diagonal element α in the dielectric tensor. For ordinary values of α in ferromagnetic materials, third-order terms of $\partial_x{}^2\partial_y H_x$ and $\partial_y{}^3 H_x$ are small and can be ignored. In consequence, the wave equation in the ferromagnetic layer is given by

$$\partial_x{}^2 H_x + \partial_y{}^2 H_x - \frac{\varepsilon_n}{\alpha\beta}\varphi\cdot\partial_y H_x + \varphi H_x = 0 \quad (\varphi = k_0{}^2\varepsilon_n - \beta^2 - \frac{k_0{}^2\alpha^2}{\varepsilon_n})\,. \tag{3-9}$$

Because of the nonzero off-diagonal elements in the dielectric tensor, the equation involves a linear term in the propagation constant β; this leads to a nonreciprocal solution to the propagation direction. The nonreciprocal solution gives a difference in absorption coefficient between forward (z-direction) and backward (-z-direction) TM waves and, therefore, gives the isolation ratio (or the difference between forward absorption and backward absorption) in the device.

To solve the wave equation numerically, we partition the domain in space using a mesh x_0, x_1,…x_p,… in x direction and mesh y_0, y_1,…y_q,… in y direction with a mesh width (the difference between two adjacent space points) of m in x direction and n in y direction. We represent the magnetic field on each mesh point (x_p, y_q) by $H_{p,q}$. Using a second-order central difference for the space derivative at position (x_p, y_q), we obtain the recurrence equation

$$\frac{1}{m^2}H_{p-1,q} + \frac{1}{m^2}H_{p+1,q} + \frac{1}{n^2}H_{p,q-1} + \frac{1}{n^2}H_{p,q+1} + (\phi - \frac{2}{m^2} - \frac{2}{n^2})H_{p,q} = 0 \tag{3-10}$$

for eq. (3-8), and recurrence equation

$$\frac{1}{m^2}H_{p-1,q} + \frac{1}{m^2}H_{p+1,q} + \frac{1}{n^2}H_{p,q-1} + \frac{\varepsilon_n}{2n\alpha\beta}\varphi H_{p,q-1} + \frac{1}{n^2}H_{p,q+1} - \frac{\varepsilon_n}{2n\alpha\beta}\varphi H_{p,q+1} + (\varphi - \frac{2}{m^2} - \frac{2}{n^2})H_{p,q} = 0 \tag{3-11}$$

for eq. (3-9). Solving eqs. (3-10) and (3-11) numerically, we can calculate the forward and backward propagation loss and the isolation ratio, as a function of the thicknesses of the cladding layer and the ferromagnetic layer, where the SOA is not operated. (In actual operation, the SOA is operated so that it compensates for the forward propagation loss.)

Before calculating the optimum thicknesses of the cladding and ferromagnetic layers, we must design the appropriate structure of the SOA region to amplify 1.5-μm TM-mode light. The structural parameters we used for the SOA was as follows. The substrate is a highly doped n-type InP (refractive index n = 3.16). The constituent layers of the SOA are: (i) lower guiding layer: 100-nm thick InGaAlAs (bandgap wavelength λ_g = 1.1 μm, n = 3.4), (ii) MQW: five InGaAs quantum wells (-0.4% tensile-strained, 15-nm-thick well, n_{MQW} = 3.53) with six InGaAlAs barriers (+0.6% compressively strained, 12-nm-thick barrier, λ_g = 1.2 μm), and (iii) upper guiding layer: 100-nm-thick InGaAlAs (λ_g = 1.1 μm, n = 3.4).

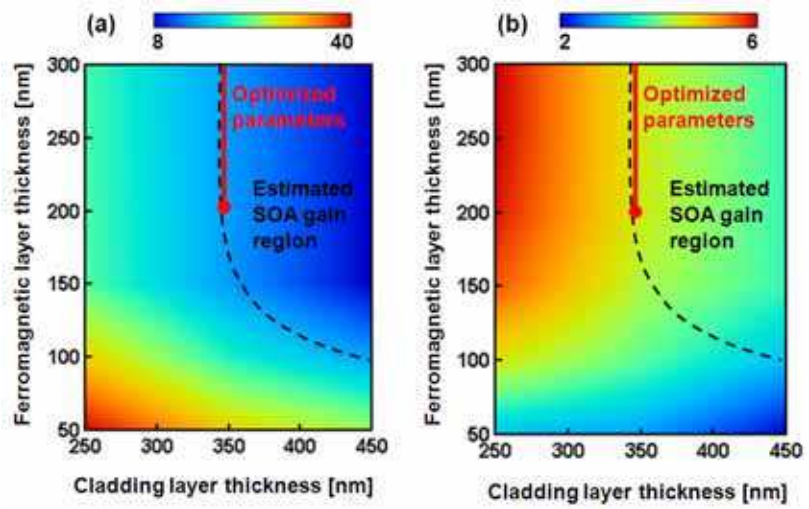

Fig. 7. (a) Forward absorption loss (propagation loss) and (b) isolation ratio (nonreciprocity) in the device as a function of Ferromagnetic-layer thickness and cladding layer thickness, calculated for 1.55-μm TM mode.

For the isolator with this SOA region, we calculated the propagation loss and the isolation ratio, using the method described above. Figure 7 shows an example of the results, i.e., (a) the absorption loss for forward propagation and (b) the isolation ratio as a function of the InP-cladding and ferromagnetic layer thicknesses. In this simulation, we assumed a device consisting of a ridge-shaped optical amplifying waveguide (see Fig. 5(b)) covered with a ferromagnetic MnAs layer and an Au-Ti metal electrode. The reason we used manganese pnictides as the ferromagnetic layer will be explained in Section 5. The parameters we used in the simulation are given in Table 1. The forward absorption loss in the device is large and the isolation ratio is small at small MnAs thickness because part of the propagating light in the device leaks out of the MnAs layer and is needlessly absorbed by the Au-Ti electrode. As MnAs layer thickness increases, forward absorption loss decreases and isolation ratio increases, both approaching a constant in MnAs layers thicker than 200 nm. This means that light penetrates to a depth of about 200 nm in the MnAs layer. Therefore, more than 200 nm can be considered a necessary and sufficient thickness for the MnAs layer when fabricating devices.

Figure 7 also shows that both the isolation ratio and the absorption loss increase as the thickness of the InP-cladding layer decreases. This is so because a thinner cladding layer lets a higher percentage of light through into the MnAs layer, producing a larger interaction. A thin cladding layer is preferable for obtaining a large isolation ratio as long as the forward absorption loss can be compensated for by the amplifying gain of the SOA. We expected an SOA gain of 16 dB/mm, and therefore decided that the optimum thickness of the cladding layer was 350 nm.

Figure 8 illustrates the distribution profile of light traveling in the isolator for forward and backward propagation, with the results calculated for a device with a 350-nm InP-cladding layer and a 200-nm MnAs layer. Figures 8(a-1) and 8(b-1) show the contour lines for TM magnetic field vector intensity—large magnetic fields in the central part—on the cross

Parameters	Values	Layers
$\varepsilon_1, \varepsilon_5$	$(3.16)^2$	InP substrate, InP cladding layer
$\varepsilon_2, \varepsilon_4$	$(3.4)^2$	InGaAsP down, upper guiding layer [a]
ε_3	$(3.53)^2$	MQW layer [b]
ε_6	$(2.8+4i)^2$	Ferromagnetic MnAs layer
ε_7	$(0.6+10i)^2$	Au/Ti metal electrode
α	$-1.62+0.27i$	Ferromagnetic MnAs layer
m	200×10^{-9}	Mesh width of x axis
n	50×10^{-9}	Mesh width of y axis

[a] The thickness of each guiding layer is fixed to 100 nm.
[b] The thickness of the MQW layer is fixed to 150 nm.

Table 1. Example of parameters used for calculating device characteristics.

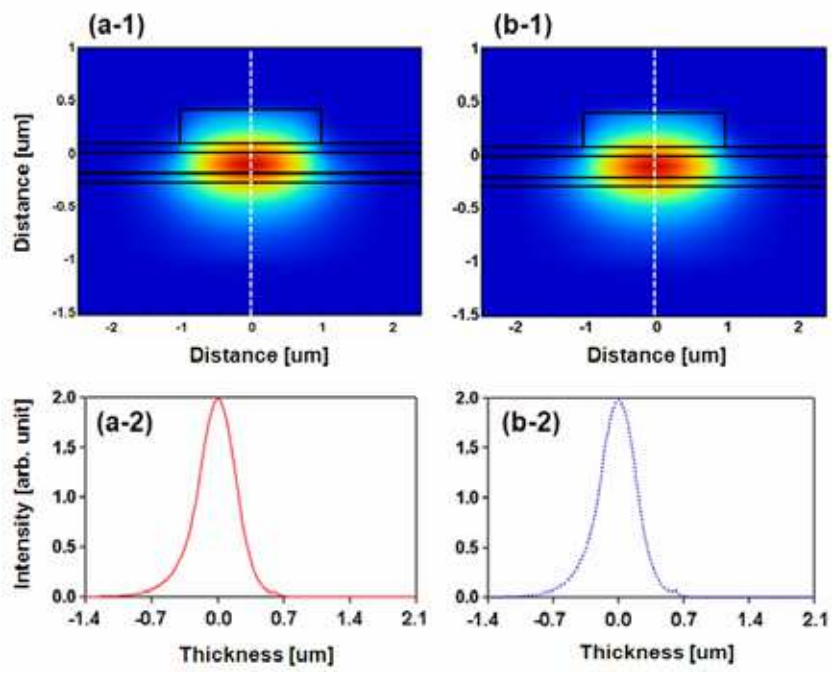

Fig. 8. Distribution profile of light traveling in isolator, calculated for 1.55 μm TM mode, with a 350-nm cladding layer and a 200-nm MnAs layer: cross section of distribution for (a-1) forward and (b-1) backward propagating light; distribution along vertical center line (dashed lines in (a-1) and (b-1)) of device for (a-2) forward and (b-2) backward propagating light.

section (*x*-*y* plane) of the device, where Fig. 8(a-1) is for forward propagating light and Fig. 8(b-1) is for backward light. Figures 8(a-2) and 8(b-2) depict the magnetic field vector intensity along the vertical center line (dashed lines in Figs. 8(a-1) and 8(b-1)) of the device, where Fig. 8(a-2) is for forward light and Fig. 8(a-2) is for backward light. Unlike forward propagating light, backward propagating light shifts its distribution tail to the MnAs layer and, therefore, suffers a larger absorption loss in the MnAs layer. Therefore, the propagation loss of light is larger in backward than in forward propagation.

5. Prototype device with ferromagnetic MnAs

5.1 Using manganese pnictides as a ferromagnetic material

The point of our device is its use of manganese arsenide (MnAs) as a ferromagnetic material, instead of ordinary ferromagnetic metals such as Fe and Co. In our device structure——which is necessary for TM-mode operation——the ferromagnetic layer used to produce the nonreciprocity is also used as a contact to supply a driving current to the SOA. This means that the ferromagnetic layer has to meet a dual requirement of (i) producing a large Kerr effect at the wavelength of 1.5 μm and of (ii) providing a low-barrier contact for p-type III-V semiconductors. Ordinary ferromagnetic metals are not suited for this purpose because they produce a Schottky barrier on III-V semiconductors, thereby producing a high-resistance contact on the contact layer. In addition, during contact annealing, they produce undesirable nonferromagnetic compounds such as FeAs and CoAs at the contact interface and simultaneously degrade the microscopic flatness of the interface; this reduces optical nonreciprocity in the device. To solve these problems, we used manganese arsenide, MnAs, for the ferromagnetic layer. MnAs are ferromagnetic, intermetallic compounds with a NiAs-type hexagonal structure (see Fig. 9). They can be grown epitaxially on GaAs, InP, and related semiconductors by means of molecular beam epitaxy (MBE), without producing a solid-phase reaction at the interface [31-34]. MnAs is suitable ferromagnetic materials for our device because they have enough Kerr effect at 1.5-μm wavelength to produce practical nonreciprocity and, at the same time, can make a low-resistance contact on III-V semiconductors. The Currie temperature is 40°C for MnAs.

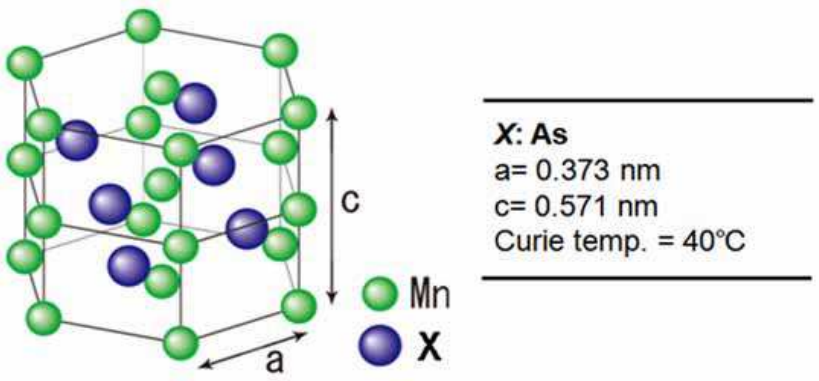

Fig. 9. Structure of manganese pnictides.

To take the first step, we made a device with a MnAs layer because the epitaxial growth technology of MnAs layers on III-V semiconductors was well established [31-33]. To reduce the propagation loss of light and obtain a single-mode operation, we used the ridge waveguide structure with a large lateral-confinement factor (see Fig. 5(b)). In the following sections, we provide details of the fabrication process and operation characteristics of the device that uses ferromagnetic MnAs.

5.2 Constructing the device

Figure 10(a) is a cross-sectional diagram of our TM-mode waveguide isolator with a ferromagnetic MnAs layer. The MnAs layer covers the SOA surface, and two interface layers (a highly doped p-type InGaAs contact layer and a p-type InP cladding layer) are inserted between the two. The InGaAs contact layer has to be thin so that 1.5-μm light traveling in the SOA will extend into the MnAs layer (the absorption edge of the contact layer is about 1550 nm). An Au/Ti double metal layer covers the MnAs layer, forming an electrode for current injection into the SOA. Light passes through the SOA waveguide in a direction perpendicular to the figure (z direction). An Al_2O_3 insulating layer separates the SOA surface from the Au-Ti electrode except on the contact region. Incident light passes through the SOA waveguide perpendicular to the figure (z direction).

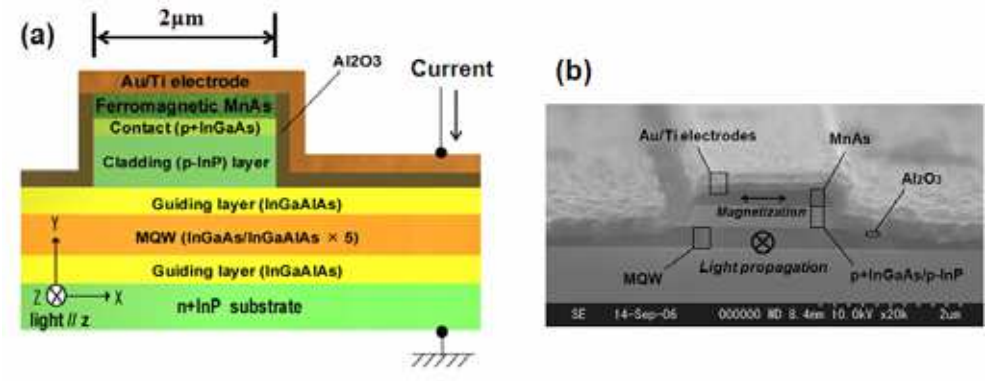

Fig. 10. (a) Schematic cross section of our waveguide isolator for 1.5-μm TM mode, consisting of a ridge-shaped optical amplifying waveguide covered with a MnAs layer magnetized in *x*-direction. Light propagates along *z*-direction. (b) SEM cross section of device.

On the basis of the simulation results mentioned in Section 4.3, we fabricated a device as follows. The substrate was a highly doped, [100]-oriented n-type wafer of InP. The SOA was formed on the substrate by metalorganic vapor-phase epitaxy (MOVPE). The MQW showed a photoluminescence peak at 1.54 μm——this means that the SOA had a gain peak at 1.54 μm. The thicknesses of the p-InP cladding and p^+InGaAs contact layers were set to be 350 nm and 10nm. After the formation of the SOA, a 200 nm MnAs layer was grown on the surface of the p^+InGaAs contact layer by MBE. The wafer was first heat treated at about 550

°C under As_2 flux in the MBE chamber to remove a native oxide layer on the contact layer. The wafer temperature was then lowered to 200°C, and the As_2 flux was kept supplying to form an As template on the surface. This As template on the surface is important to grow high quality MnAs, as in the growth of MnAs layers on GaAs [31, 32] and InP [33]. The surface of the InGaAs contact layer with the As template showed spotty refraction high energy electron diffraction (RHEED) pattern. After that, Mn and As_2 fluxes were supplied on the surface to grow a 200 nm MnAs thin film. During the growth process, we confirmed (1×2) reconstruction in RHEED, indicating that the MnAs structural properties were improved. An X-ray diffraction pattern showed strong MnAs peaks in [1-100] directions.
After the growth of MnAs, the ridge waveguide structure was formed as follows. First, a photoresist mask in the form of a 2-μm-wide waveguide pattern was made on the surface of the MnAs layer. Then, the MnAs layer, InP cladding layer, and InGaAs contact layers were selectively etched in this order to fabricate a ridge waveguide—the MnAs layer was etched by reactive ion etching with Ar, and the cladding and the contact layers were wet-etched with a Br_2-HBr-H2O solution. An Al_2O_3 layer was deposited on this ridge waveguide using electron-beam (EB) evaporation. Then, the Al_2O_3 on the contact layer was removed using a lift-off process. Finally, a Ti layer and an Au layer were deposited to make a top electrode, using EB evaporation. This was the process we used to fabricate the structure depicted in Fig. 10(a). Finally, both ends of the device were cleaved, and the cleaved surfaces were left uncoated. Figure 10(b) is a cross section of the device as observed with scanning electron microscopy (SEM).

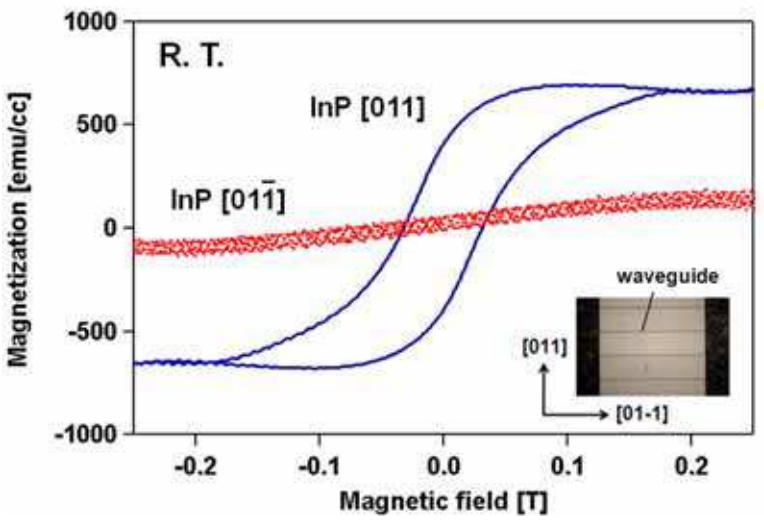

Fig. 11. Magnetization curve for MnAs layer, measured with a AGFM. MnAs layer can be easily magnetized along [011] direction of InP substrate. In contrast, magnetization is difficult along [01-1] direction.

MnAs thin films grown on the InGaAs contact layer showed strong magnetocrystalline anisotropy——an intrinsic property of a ferrimagnet, independent of grain size and shape; the MnAs thin films were easily magnetized along the [011] direction of the InP substrates. Based on the fact, we formed the waveguide stripe parallel to the [0-11] direction of the InP substrate, and applied an external magnetic field to the [011] direction (x-direction in Fig. 10). However, in addition to the magnetocrystalline anisotropy, the shape anisotropy of the MnAs layer must be taken into consideration for the fabricated device because our device (or the MnAs layer) had the form of the 2-μm-wide waveguide structure. Therefore, we confirmed a magnetization curve of the MnAs layer in our device before measuring device characteristics. Figure 11 shows a plot of the magnetization curve, measured by alternating gradient force magnetometry (AGFM). Along the [011] direction of the InP substrate, the MnAs layer showed a soft hysteresis curve and was easily magnetized with a small coercive field of 0.07 T. In contrast, the magnetization was not easy along the [01-1] direction and was insufficient even in a magnetic field of 0.5 T. This means that the magnetocrystalline anisotropy is larger than the shape anisotropy in our device, and the device was expected to work with an external magnetic field of 0.07-0.1 T (initial magnetizing requires 0.15-0.2 T).

5.3 Device operation

We confirmed that the device functioned successfully as an optical isolator with nonreciprocal loss for TM-polarized, 1.5-μm light. Figure 12 shows our experimental setup for the measurement. It consisted of a wavelength-tunable laser, two polarization controllers, two circulators, two optical switches, an output coupler, an optical power meter, and an optical spectrum analyzer (OSA). Light from a tunable laser was transmitted to the device through a polarization controller and a circulator. The light was transferred into and out of the device using lensed-fiber couplers. A magnetic field was applied using a permanent magnet along the [011] direction of the device, i.e., parallel to the surface of the device and perpendicular to the direction of light propagation. Light propagation in the device was switched between forward direction (switch node 1–upper circulator–device–lower isolator– switch node 4 in Fig. 12) and backward direction (node 2–lower circulator–

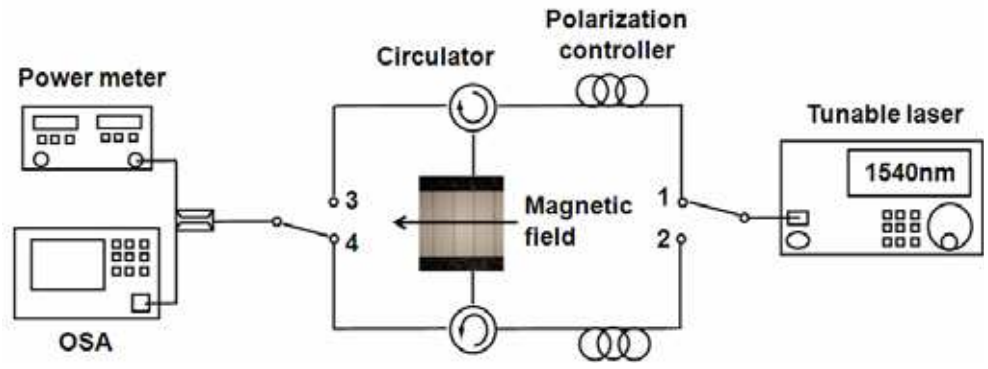

Fig. 12. Experimental setup for measuring isolation ratio and propagation loss of light in device.

device–upper isolator–node 3) by controlling the optical switches. The intensity of light transmitted in the device (or the output light from the device) was measured using the optical spectrum analyzer and the power meter. The output of the tunable laser was set to 5 dBm, and the magnetic field for the device was set to 0.1 T. During measurement, the device was kept at 20°C and operated with a SOA driving current of 100 mA. The MnAs layer successfully provided a low-resistance contact for the InGaAs contact layer. The voltage drop across the device 0.65 mm in length was only 1.7 V (SOA diode drop 0.9 V plus ohmic contact drop 0.8 V), whereas the drop across a control device with Fe-Ni layers instead of MnAs was 3.0 V (SOA diode drop 0.9 V plus ohmic contact drop 2.1 V) [35].

Figure 13 shows the transmission spectra of the device with a length of 0.65 mm. The intensity of the output light from the device is plotted as a function of wavelength for forward (dashed line) and backward (solid line) propagation of (a) TM-polarized and (b) TE-polarized light. The wavelength of incident light was fixed at 1.54 μm, which was the gain peak wavelength of the SOA. For TM-mode light, the output intensity changed by 4.7 dB by switching the direction of light propagation. The device operated efficiently as a TM-mode isolator with an isolation ratio of 7.2 dB/mm (= 4.7 dB/0.65 mm). In contrast, the output intensity for TE-mode light was not dependent on the direction of the light propagation. Small periodic ripples in amplified spontaneous emission spectra are shown in Fig. 13. They are caused by Fabry-Perot interference due to reflection from cleaved facets; the period was consistent with the value predicted from the length and effective refractive index of the device. The inset in Fig 13(a) is the near-field pattern of the TM-mode forward propagating light and shows that the device operated successfully in a single mode.

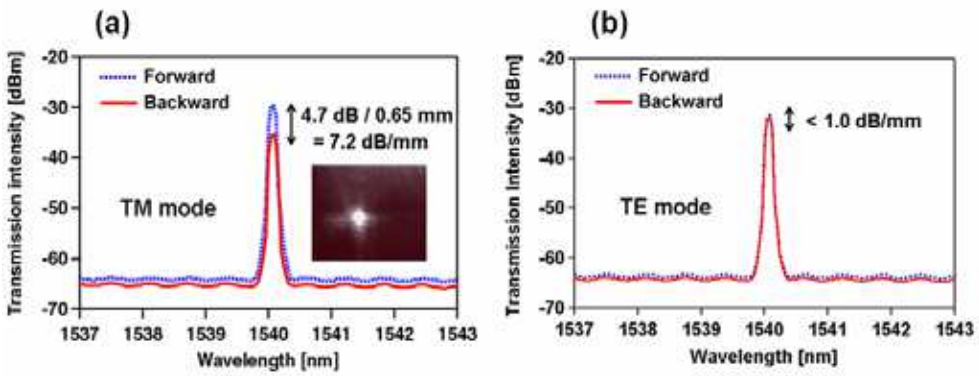

Fig. 13. Transmission spectra of device for forward transmission (dashed line) and backward transmission (solid line), measured for (a) TM-mode and (b) TE-mode, at 1.54-μm wavelength, 100-mA driving current, and 0.1-T magnetic field. Device is 0.65 mm long. Data on transmission intensity include loss caused by measurement system. Inset is near-field pattern of TM-mode forward propagating light.

The data of transmission intensity in Fig. 13 include the loss caused by the measurement system. To examine the intrinsic transmission loss of the device, we measured the transmission intensity for devices with different lengths. Figure 14 shows the results, i.e., the output intensity for forward and backward transmission as a function of device length (isolation ratio is also plotted). The slope of the forward line gives the intrinsic transmission loss (or absorption loss) per unit length. We estimated that forward loss in the device was 10.6 dB/mm—still large for practical use. This is so because the gain of the SOA was lower than we had expected, and therefore, insufficient to compensate for the intrinsic transmission loss in the device. The loss caused by the measurement system can also be calculated using the vertical-axis intercept of the forward line and the output intensity of the tunable laser. It was estimated to be 28 dB—output coupler loss 3 dB plus lensed-fiber coupling loss 12.5 dB/facet × 2 between the measurement system and the device.

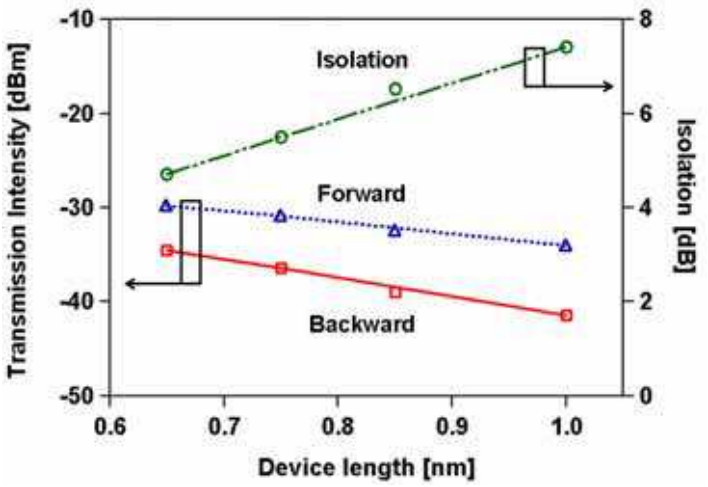

Fig. 14. Transmission intensity as a function of device length, measured for 1.54 μm TM mode, with 100-mA driving current and 0.1-T magnetic field. Isolation ratio is also plotted.

Figure 15 is a plot of the isolation ratio, as a function of wavelength from 1.53 to 1.55 μm. The device was 0.65-mm long. The output intensities for forward and backward propagations are also plotted (including the measurement system loss). In this range of wavelength, the isolation ratio was almost constant. The isolation ratio 7.2 dB/mm of this waveguide isolator was still small for practical use. In addition, the device was unable to operate at temperatures higher than room temperature because the Currie temperature of MnAs is only 40°C. To improve the device performance, we have to seek other superior ferromagnetic materials. In the next section, we present a device that uses MnSb instead of MnAs.

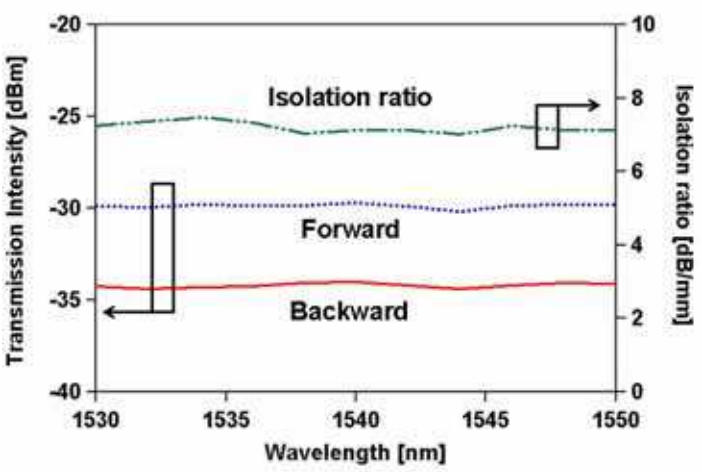

Fig. 15. Isolation ratio as a function of a wavelength from 1.53 to 1.55 μm for a 0.65-mm long device. Transmission intensity is also plotted for forward and backward propagation (including measurement system loss).

6. Conclusion

An important element for developing photonic integrated circuits is waveguide optical isolators that can be monolithically combined with other waveguide-based devices such as lasers. One promising way of creating such waveguide isolators is by using the phenomenon of nonreciprocal loss in magneto-optical waveguides. Making use of this phenomenon, we have been developing TE- and TM-mode waveguide isolators operating at 1.5-μm telecommunication band. As a fromagnetic material for the magneto-optical waveguide isolator, manganese pnictides such as MnAs are more superior than ordinary ferromagnetic metals because they can be formed on GaAs, InP, and related materials using semiconductors manufacturing process. Although MnAs is not common material at present for integrated optics, it will soon bring technical innovation in functional magneto-optic devices for large-scale photonic integrated circuits.

7. References

[1] O. Wada; T. Sakurai; T. Nakagami IEEE J. Quantum Electron. 1986, 22, 805-821.
[2] T. L. Koch; U. Koren IEEE J. Quantum Electron. 1991, 27, 641-653.
[3] A. A. M. Staring; L. H. Spiekman; J. J. M. Binsma; E. J. Jansen; T. van Dongen; P. J. A. Thijs; M. K. Smit; B. H. Verbeek IEEE Photon. Technol. Lett. 1996, 8, 1139-1141.
[4] Nagarajan, R.; Joyner, C.H.; Schneider, R.P., Jr.; Bostak, J.S.; Butrie, T.; Dentai, A.G.; Dominic, V.G.; Evans, P.W.; Kato, M.; Kauffman, M.; Lambert, D.J.H.; Mathis, S.K.; Mathur, A.; Miles, R.H.; Mitchell, M.L.; Missey, M.J.; Murthy, S.; Nilsson, A.C.;

Peters, F.H.; Pennypacker, S.C.; Pleumeekers, J.L.; Salvatore, R.A.; Schlenker, R.K.; Taylor, R.B.; Huan-Shang Tsai; Van Leeuwen, M.F.; Webjorn, J.; Ziari, M.; Perkins, D.; Singh, J.; Grubb, S.G.; Reffle, M.S.; Mehuys, D.G.; Kish, F.A.; Welch, D.F. IEEE J. Select. Topics Quantum Electron. 2005, 11, 50-65.

[5] N. Sugimoto; H. Terui; A. Tate; Y. Katoh; Y. Yamada; A. Sugita; A. Shibukawa; Y. Inoue J. Lightwave Technol. 1996, 14, 2537-2546.

[6] M. Levy; R. M. Osgood; H. Hegde; F. J. Cadieu; R. Wolfe; V. J. Fratello IEEE Photonics Technol. Lett. 1996, 8, 903-905.

[7] M. Fehndrich; A. Josef; L. Wilkens; J. Kleine-Börger; N. Bahlmann; M. Lohmeyer; P. Hertel; H. Dötsch Appl. Phys. Lett.1999, 74, 2918-2920.

[8] J. Fujita; M. Levy; R. M. Osgood; L. Wilkens; H. Dotsch Appl. Phys. Lett. 2000, 76, 2158-2160.

[9] M. Levy IEEE J. Sel. Top. Quantum Electron. 2002, 8, 1300-1306.

[10] J. S. Yang; J. W. Roh; S. H. Ok; D. H. Woo; Y. T. Byun; W. Y. Lee; T. Mizumoto; S. Lee IEEE Trans. Magn. 2005, 41, 3520-3522.

[11] T. R. Zaman; X. Guo; R. J. Ram IEEE Photonics Technol. Lett. 2006, 18, 1359-1361.

[12] http://www.namiki.co.jp/

[13] K. Ando; N. Takeda; N. Koshizuka; T. Okuda J. Appl. Phys. 1985, 57, 1277-1281.

[14] H. Dammann; E. Pross; G. Rabe; W. Tolksdorf; M. Zinke Appl. Phys. Lett. 1986, 49, 1755-1757.

[15] B. M. Holmes; D. C. Hutchings Appl. Phys. Lett. 2006, 88, 061116.

[16] B. M. Holmes; D. C. Hutchings Proc. of IEEE Lasers and Electro-Optics Society 2006, 897-898.

[17] H. Yokoi; T. Mizumoto; N. Shinjo; N. Futakuchi; Y. Nakano Appl. Optics 2000, 39, 6158-6164.

[18] H. Yokoi; T. Mizumoto; Y. Shoji Appl. Optics 2003, 42, 6605-6612.

[19] K. Sakurai; H. Yokoi; T. Mizumoto; D. Miyashita; Y. Nakano Jpn. J. Appl. Phys. 2004, 43, 1388-1392.

[20] Y. Shoji; T. Mizumoto Appl. Optics 2006, 45, 7144-7150.

[21] M. Vanwolleghem; W. Van Parys; D. Van Thourhout; R. Baets; F. Lelarge; O. Gauthier-Lafaye; B. Thedrez; R. Wirix-Speetjens; and L. Lagae Appl. Phys. Lett. 2004, 85, 3980-3982.

[22] W. Van. Parys; B. Moeyersoon; D. Van. Thourhout; R. Baets; M. Vanwolleghem; B. Dagens; J. Decobert; O. L. Gouezigou; D. Make; R. Vanheertum; L. Lagae Appl. Phys. Lett. 2006, 88, 071115.

[23] H. Shimizu; Y. Nakano Jpn. J. Appl. Phys. 2004, 43, L1561-L1563.

[24] H. Shimizu; Y. Nakano IEEE J. Lightwave Technol. 2006, 24, 38-43.

[25] T. Amemiya; H. Shimizu; Y. Nakano; P. N. Hai; M. Yokoyama; M. Tanaka Appl. Phys. Lett. 2006, 89, 021104.

[26] T. Amemiya; H. Shimizu; P. N. Hai; M. Yokoyama; M. Tanaka; Y. Nakano Appl. Optics 2007, 46, 5784-5791.

[27] W. Zaets; K. Ando Appl. Phys. Lett. 2000, 77, 1593-1595.

[28] V. Zayets; M. C. Debnath; K. Ando Appl. Phys. Lett. 2004, 84, 565-567.

[29] M. Takenaka; Y. Nakano Proc. of IEEE Conference on Indium Phosphide and Related Materials 1999, 289-292.
[30] W. Zaets; K. Ando IEEE Photonics Technol. Lett. 1999, 11, 1012-1014.
[31] M. Tanaka; J. P. Harbison; G. M. Rothberg Appl. Phys. Lett. 1994, 65, 1964-1966.
[32] L. Daweritz; L. Wan; B. Jenichen; C. Herrmann; J. Mohanty; A. Trampert; K. H. Ploog J. Appl. Phys. 2004, 96, 5052-5056.
[33] M. Yokoyama; S. Ohya; M. Tanaka Appl. Phys. Lett. 2006, 88, 012504.
[34] H. Akinaga; K. Tanaka; K. Ando; T. Katayama J. Cryst. Growth 1995, 150, 1144-1149.
[35] T. Amemiya; H. Shimizu; Y. Nakano, Proc. of IEEE Conference on Indium Phosphide and Related Materials 2005, 303-306.
[36] Y. Ogawaa; T. Amemiya; H. Shimizu; Y. Nakano; H. Munekata Proc. of International Symposium on Compound Semiconductors 2007, TuC-P22.

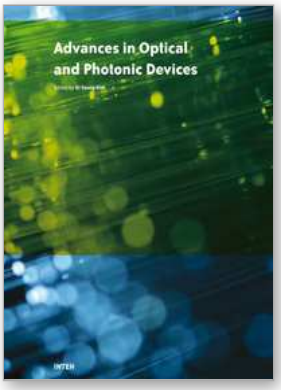

Advances in Optical and Photonic Devices

Edited by Ki Young Kim

ISBN 978-953-7619-76-3
Hard cover, 352 pages
Publisher InTech
Published online 01, January, 2010
Published in print edition January, 2010

The title of this book, Advances in Optical and Photonic Devices, encompasses a broad range of theory and applications which are of interest for diverse classes of optical and photonic devices. Unquestionably, recent successful achievements in modern optical communications and multifunctional systems have been accomplished based on composing “building blocks” of a variety of optical and photonic devices. Thus, the grasp of current trends and needs in device technology would be useful for further development of such a range of relative applications. The book is going to be a collection of contemporary researches and developments of various devices and structures in the area of optics and photonics. It is composed of 17 excellent chapters covering fundamental theory, physical operation mechanisms, fabrication and measurement techniques, and application examples. Besides, it contains comprehensive reviews of recent trends and advancements in the field. First six chapters are especially focused on diverse aspects of recent developments of lasers and related technologies, while the later chapters deal with various optical and photonic devices including waveguides, filters, oscillators, isolators, photodiodes, photomultipliers, microcavities, and so on. Although the book is a collected edition of specific technological issues, I strongly believe that the readers can obtain generous and overall ideas and knowledge of the state-of-the-art technologies in optical and photonic devices. Lastly, special words of thanks should go to all the scientists and engineers who have devoted a great deal of time to writing excellent chapters in this book.

How to reference

In order to correctly reference this scholarly work, feel free to copy and paste the following:

T. Amemiya and Y. Nakano (2010). Single Mode Operation of 1.5-μm Waveguide Optical Isolators Based on the Nonreciprocal-loss Phenomenon, Advances in Optical and Photonic Devices, Ki Young Kim (Ed.), ISBN: 978-953-7619-76-3, InTech, Available from: http://www.intechopen.com/books/advances-in-optical-and-photonic-devices/single-mode-operation-of-1-5-micro-m-waveguide-optical-isolators-based-on-the-nonreciprocal-loss-phe

INTECH
open science | open minds

InTech Europe
University Campus STeP Ri
Slavka Krautzeka 83/A
51000 Rijeka, Croatia

InTech China
Unit 405, Office Block, Hotel Equatorial Shanghai
No.65, Yan An Road (West), Shanghai, 200040, China
中国上海市延安西路65号上海国际贵都大饭店办公楼405单元

Phone: +385 (51) 770 447
Fax: +385 (51) 686 166
www.intechopen.com

Phone: +86-21-62489820
Fax: +86-21-62489821

© 2010 The Author(s). Licensee IntechOpen. This chapter is distributed under the terms of the Creative Commons Attribution-NonCommercial-ShareAlike-3.0 License, which permits use, distribution and reproduction for non-commercial purposes, provided the original is properly cited and derivative works building on this content are distributed under the same license.